Dependence of CO oxidation on Pt nanoparticle shape: A shape-selective approach to the synthesis of PEMFC catalysts

ARTICLE *in* APPLIED ORGANOMETALLIC CHEMISTRY · JANUARY 2008

Impact Factor: 2.25 · DOI: 10.1002/aoc.1349

Research Article

Applied Organometallic Chemistry

Received: 17 August 2007 Revised: 10 October 2007 Accepted: 14 October 2007 Published online in Wiley Interscience: 18 December 2007

(www.interscience.com) DOI 10.1002/aoc.1349

Dependence of CO oxidation on Pt nanoparticle shape: a shape-selective approach to the synthesis of PEMFC catalysts

Sachin Kinge[a†], Christian Urgeghe[b*], Achille De Battisti[b] and Helmut Bönnemann[a]

In real catalyst systems, it is difficult to establish a correlation between catalytic properties and the shape (crystal planes, corners and steps) of the active catalytic particles. In this paper we present a clear shape dependence of the catalytic properties of a Vulcan-supported fuel cell catalyst having 4 nm cubo-octahedral platinum(0) nanocrystallites with (111) and (100) surfaces stabilized by sodium polyacrylate. The electrode materials were characterized by CO-stripping cyclic voltammetry and transmission electron microscopy (TEM), showing that no agglomeration had occurred among the nanoparticles on the catalyst surfaces. Copyright © 2007 John Wiley & Sons, Ltd.

Keywords: PEM; PEMFC catalysts; CO-oxidation; shape-selective particle preparation

Introduction

The catalytic properties of nanocrystallites depend upon their shape – specifically on the nature and distribution types and numbers of crystal planes, edges, corners and steps.[1–4] Changes in the crystal shape alter the relative numbers and types of facets, the relative numbers of atoms located on the corners or edges of the crystals, and the total number of atoms exposed on the surface and their coordination numbers. For example, the proportion of atoms located on the edges and corners is greatest for tetrahedral particles, and this could confer a higher activity upon nanoparticles with this geometry. Further, the control of particle size and the kinetics of their growth are directly related to their catalytic activity due to changes in the adsorption energies or transition state energies.[5] Several significant studies have been devoted to size-dependent properties of nanoparticles.[6–11] Shape selectivity studies on nanoparticles fall into the realm of surface science, and surface-dependent properties have been extensively investigated on single crystal surfaces in ultra-high vacuum (UHV) conditions. Shape selectivity studies of real catalysts with geometrically defined nanocrystalline particles, however, are rare because these are not easily accessible.[6–11] Here we exploit the shape- and size-selective particle synthesis for the development of highly active polymer electrolyte membrane fuel cell/direct methanol fuel cell (PEMFC/DMFC) catalysts, which is a major challenge for the catalysis community today. The efficiency of catalysts based on mono-, bi- and multi-metallic Pt colloids for FC applications is being investigated.[12,13] The dependence of CO oxidation on different crystal surfaces has been previously studied in UHV surface science.[14–16] While most efforts in real fuel cell (FC) systems are devoted to studying the size selectivity of polycrystalline nanocatalysts of different sizes, no study on shape dependence has been reported.[17] However, we consider that the key to optimizing electrode catalysis is the study of model catalyst systems that have a well-controlled composition of their surfaces defined by surface analytical techniques.[18]

Although new synthetic approaches for tailoring the size and shape of nanoparticles continue to be the subject of intense investigation, it remains a challenge to synthesize nanoparticles within well-defined geometric constraints. Recently, we developed a different approach to controlling the form of Pt nanoparticles by employing an external seeding method. This offers better and wider control over the size and shape of the nanocrystallites[19] and about 90% of the platinum nanoparticles in samples prepared in this way have a truncated octahedral shape. Details of the preparative method have been described elsewhere.[19,20] For the studies reported here we used this 'seeding method' to synthesize cubo-octahedral Pt(0) nanoparticles with an average size of 4 nm with well-defined (111) and (100) surfaces and examined the shape dependence of CO oxidation on them.

These uniform particles were supported on Vulcan XC-72 in 20% weight. Cyclic voltammetric studies of CO oxidation on this catalyst show the presence of two peaks which can be assigned to two different sites of CO oxidation, i.e. two different crystal surfaces, (111) and (100). Further, since TEM analysis after repeated cyclic voltammetric studies shows that no agglomeration had taken place, any effects due to the coalescence of nanoparticles can be excluded. This is important as such effects could improve or degrade the overall catalytic efficiency of the fuel cell.

* *Correspondence to: Christian Urgeghe, Dipartimento di Chimica, via L. Borsari 46, 44100, University of Ferrara, Ferrara Italy. E-mail: rggcrs@unife.it*

† *Present address: Supramolecular Chemistry and Technology, TNW, PO Box 217, MESA+ Institute for Nanotechnology, 7500 AE, Enschede, The Netherlands.*

a *MPI für Kohlenforschung, Mülheim an der Ruhr, D-45470 Germany*

b *Dipartimento di Chimica, via L. Borsari 46, 44100, University of Ferrara, Ferrara, Italy*

Experimental

Synthesis of Pt nanoparticles

Small truncated- or cubo-octahedral Pt nanoparticles were synthesized by the seeding method,[19] essentially a modified El-Sayed method.[20] Pre-prepared Pt particles of 1 nm size[21] have been used as the seed to grow larger nanoparticles in a shape-selective way. These seeds are added at approximately 5 wt% to the precursor solution containing K_2PtCl_4 (1 mmol) and Na polyacrylate (1 mmol) in 1 : 1 proportion. The resulting aqueous solution was purged with hydrogen (typical hydrogen flow 10 l h^{-1}) to reduce the precursors completely. After stirring overnight, a furnace black, Vulcan XC-72 (Cabot Co.), was added to the reduced black solution to attain a loading of 20 wt% Pt on Vulcan. Surfactant was removed by repeated addition of acetonitrile (50 ml) to the aqueous solution. Solvents were pumped off by freeze-drying. The resultant free-flowing catalyst powder was suspended in 'Milli-Q' water for electrochemical studies. TEM analyses of these particles show monodisperse 4 nm cubo-octahedral particles (Fig. 1). TEM analyses were performed with a Hitachi H7500 instrument (magnification up to 1.25×10^6) operating at 200 kV acceleration voltage. For TEM analyses the specimens were prepared by placing a drop of the material under investigation in water on a carbon film covered with a nickel grid and evaporating the solvent. The determination of the shape and size distribution of the Pt particles was based on 300 particles taken from three different frames.

Electrochemical measurements

All electrochemical measurements were performed using a standard three-electrode electrochemical cell with a PAR 273 potentiostat (Pine Instruments). Potentials were measured using a mercury–mercurous sulfate–K_2SO_4(sat) reference (MSE) electrode; however, all potentials are reported with respect to the normal hydrogen electrode (NHE) throughout the paper. The working electrodes were assembled as indicated below using glassy carbon disk electrodes (4 mm diameter, 0.1256 cm^2, Sigradur G from Hochtemperatur Werkstoffe GmbH). Before each electrode was prepared, the graphitic support was polished to a mirror-like surface using alumina (0.05 μm, Buehler). A platinum plate served as counter-electrode. All the data were recorded within the potential range 0.1–0.9 V NHE and their potentiodynamic response in the supporting electrolyte remained unchanged after electrochemical cycles.

Sulfuric acid solution was prepared from 'Milli-Q' water and the highest purity sulfuric acid available (Merck suprapure). Sulfuric acid was chosen because, even after taking into account complications caused by the specific adsorption of SO_4^{2-} anions in this electrolyte, it was easier to compare the results with other data from the literature.

All solutions were initially purged with Ar (6.0) (Messer–Griesheim) to remove oxygen and other volatile component from the solution. The carbon monoxide used for CO stripping measurements was CO (4.7) (Matheson).

Electrode preparation

Electrodes were prepared as described in Motte *et al.*[9] A suspension of 0.625 mg of catalyst (20% Pt loading on Vulcan XC-72) per ml of Milli-Q water was ultrasonically dispersed for 15 min. To minimize the capacitive effect of the support, a 14 μl aliquot was immediately pipetted onto the graphite surface of the glassy carbon disk electrode. The nominal loading was 14 μg_{Pt} cm^{-2}. The dispersion was desiccated under a gentle flux of argon and then the catalyst was covered with 15 μl of a Nafion solution (commercial Nafion solution, Aldrich 5 wt%, diluted with ultrapure water and

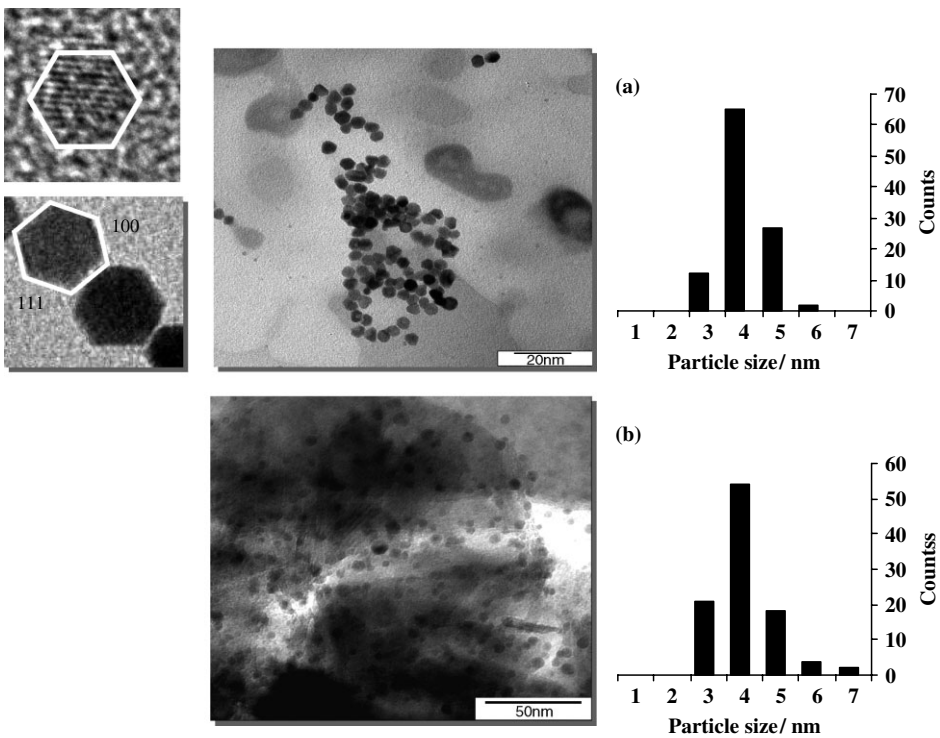

Figure 1. a): TEM of cubo-octahedral particles, av. size 4 nm, (b). *Ex-situ* TEM after electrochemistry.

isopropyl alcohol) in order to attach the catalyst particles to the electrode surface after evaporating the solvent by a stream of argon. The resulting Nafion film assures the mechanical stability: as demonstrated by a previous experiment, film diffusion effects are negligible.[22,23] No loss of activity was observed in the course of acquiring the entire family of curves, indicating the high level of electrolyte purity.

After immersion in the deaerated electrolyte, the electrode was cycled in the potential range between 0 and 0.9 V in order to make the double-layer environment uniform. It is necessary to restrict the potential to this range to avoid the transition from 'ordered' to 'disordered' Pt(111) and Pt(100) crystal surfaces as a result of the irreversible formation of oxides.[24] After the electrochemical measurements had been completed, the electrodes were examined by *ex-situ* TEM, but no evidence of agglomeration was found [see Fig. 1(b)]. Unfortunately, the images were not recorded in the same quality as those of the catalyst at the beginning, so that there remains an element of uncertainty on whether some limited agglomeration had occurred. In practice it is not an easy task to remove the catalysts from the glassy carbon disks and wash out the Nafion residues completely.

To obtain a CO-saturated monolayer before each CO stripping voltammetric experiment, CO was passed through the solution for 1000 s while maintaining the potential at 0.1 V NHE and then the excess was removed by purging the solution with Ar for 1800 s (the solubility of CO in acid media is around 10^{-3} M). It has been demonstrated that, if carbon monoxide remains in the solution, it can cause unpredictable changes in the shape of the cyclic voltammograms depending on the time elapsed between the end of the Ar purging procedure and the measurement.[25] Again, spectral features for CO ad-layers have been proved to be related to the adsorption pattern and are coverage-dependent.[26] For this kind of situation the term 'compressed' has been coined.

Results and Discussion

Base voltammetry

Figure 2 shows the base voltammogram of an electrode with Pt loading of 14 μg Pt cm^{-2}. As is well established in the literature, the shape of the cyclic voltammogram of these Pt nanocrystallites is different from that of polycrystalline Pt[27] as a result of the higher double layer capacity due to the carbon-support – this can mask other aspects of the H-adsorption/desorption behaviour. Another relevant factor is uniformity of the crystal domain.

As the particles become ever smaller, it becomes increasingly difficult to correlate the signals with their geometrical shape. In this case the particle size is around 4 nm, a region in which quantum size effects are limited.[28] From the images it is possible to recognize a cubo-octahedral shape, mainly terminated by (111) facets with additional (100) facets and low-coordination Pt atoms at corner and edge sites. (For a pictorial representation see Ross.[18] For an average Pt particle with a diameter of 3.8 nm the average distribution over the whole surface amounts to ~65% (111) terrace sites, 22% corner and edge sites, and 13% (100) terrace sites.[29])

In the H-adsorption/desorption region it is possible to observe the typical pattern of anion adsorption on large and well-ordered terraces as reported, for example, in Nart and Vielstich.[30] To calculate the number of Pt surface atoms we used the coulombic charge for hydrogen adsorption, $Q_H = (Q_{total} - Q_{DL})$, as described in literature, taking 209 μC cm^{-2} per H_{upd} monolayer), where Q_{total} is the total cathodic charge between 0.05 and 0.5 V NHE and

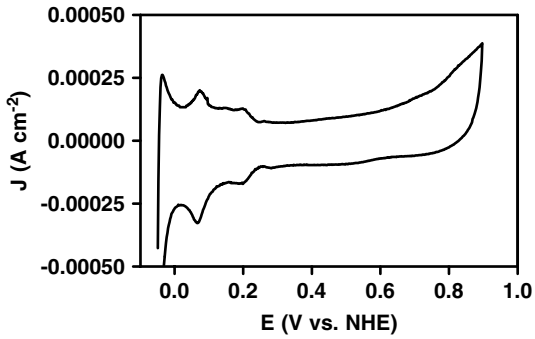

Figure 2. Cyclic voltammograms of Pt-based catalyst,supported on Vulcan XC-72 recorded in 1 M H_2SO_4 solution purged with argon, 100 mV s^{-1}.

Q_{DL} represents the capacitive charge in the double layer region and the capacitance of the high-surface-area carbon support.[30] The surface area calculated in this manner is around 30 m^2 $g^{-1}{}_{Pt}$ and the Pt surface concentration is 9.3×10^{-9} mol_{Pt} cm^{-2} (using $F = 96485$ C mol^{-1}, one-electron discharge). However, since the H_{upd} charge cannot be determined with much certainty, it is better to estimate the real surface area by measuring the capacitance associated with the CO stripping. To take into consideration the capacitive contributions due to bisulfate anions (around 80 μC cm^{-2}) and to the adsorption of OH^- (around 15 μC cm^{-2})[31] we subtracted from the CO-stripping voltammogram the one recorded immediately afterwards and used 484 μC cm^{-2} as capacitive contribution[32] per CO monolayer (in the absence of other information about the saturation at the surface). The Pt area calculated in the previous way is 23 m^2 $g^{-1}{}_{Pt}$; this value has been used to refer the current densities to a square centimeter of Pt.

CO-stripping voltammetry

CO-stripping voltammetry, a very useful and rapid method to determine the activity of electrocatalysts, uses a linear potential ramp to oxidatively remove an adsorbed monolayer of CO molecules: the resulting stripping peak potential is taken as a measure of the electrode activity. CO is normally chosen as the probe molecule because it is the simplest C1 molecule and is a common intermediate in the catalytic electrooxidation of several organic compounds. The ability of CO to act as a ligand to noble metals is important in fuel cell catalysis. The poisoning of Pt FC electrodes at low temperature lowers the overall efficiency of PEMFC and DMFC. The CO is so strongly adsorbed that it can only be removed by applying a high positive potential to the electrode surface.

The distribution and number of CO-stripping peaks can provide a large amount of information about the reactions to be catalysed. Cyclic voltammetry experiments and perturbing potential programs, together with *in-situ* reflection spectroscopy techniques,[33] particularly in the infrared region, have shown that the electro-desorptive behaviour of CO residues depends on a number of factors including the adsorption potential, electrolyte composition, scan rate, temperature, oxygen content in solution, potential limits and surface morphology.[34] It is easy to control some of these experimentally, but the average surface morphology of the nanoparticles usually changes only gradually from sample to sample, making it impossible to recognize or deduce any well-defined relationships between particle morphology and catalyst properties from cyclic voltammetry.

Figure 3 shows the CO-stripping voltammetry plot for our catalyst at a CO adsorption potential of 0.1 V. The curve is recorded

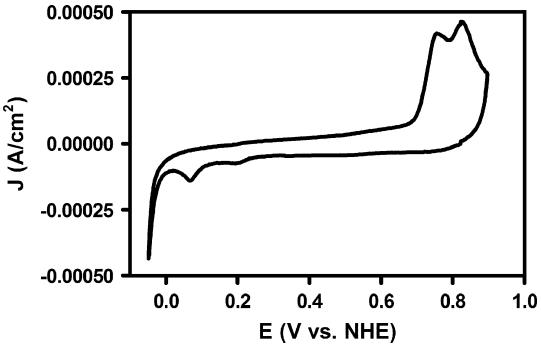

Figure 3. CO stripping Voltammetry of Pt-based catalyst, supported on Vulcan XC-72, in 1 MH_2SO_4 solution purged with argon, 100 mV s^{-1}. CO was adsorbed at 0.1 V vs. NHE which was also the initial limit.

at 100 mV s^{-1}. It should be noted that CO adsorption blocks the Pt surface completely for H-atom electrosorption and suppresses the hydrogen electrode reaction (in 0.5 M sulfuric acid approximately 0.0–0.3 V NHE). It is also easy to recognize two different peaks, one centred at 0.725 V and the other one at 0.82 V vs NHE.

One of the earliest instances where this pattern was observed in well-characterized metals and alloys is found in the work of Gasteiger *et al.*,[35] but they did not attempt to interpret it since their aim was to explain the mechanistic features of oxidation. Many other papers attribute the different experimental responses to site-specific adsorptions.[36] However, until now, no study has been reported that distinguishes between different types of adsorptive behaviour during cyclic voltammetry in a conclusive manner. While on the one hand this is understandable because the catalysts studied in the past have shown in contact with liquid phases a certain degree of CO-mobility after adsorption (see Maillard *et al.*[17] and literature cited therein) or a tendency to agglomerate,[37] on the other hand this lack is somewhat remarkable because cyclic voltammetry is usually a very powerful tool to provide this kind of information. We have tried here to clarify the origin of these peaks based upon geometrical and morphological data of Pt nanoparticles.

In our case, *ex-situ* TEM measurements on the Pt nanoparticles in the catalyst have shown that no agglomeration is present [see Fig. 1(b)]. Cyclic voltammetry experiments carried out at different scan rates indicated that on the time scale of our experiment there are some migratory effects (see Fig. 4). In effect, if the adsorbed species are able to move on the surface, then decreasing the scan rate during cyclic voltammetric experiments offers the system more time to relax or vice versa. In other words, the changes in the relative peak areas are clearly visible in agreement with the different sweep rates (the reader may find it easier to follow the peak heights), simply assuming that some of the CO molecules can move from the sites at higher energy of oxidation to the sites of lower energy if the measurement time is long enough to allow this transfer to occur.

This hypothesis was confirmed by an experiment carried out (at 100 mV s^{-1}, see Fig. 5) by stopping the potential scans. To unambiguously confirm that the two peaks at 0.725 and 0.82 V are attributable at two energetically distinguishable adsorption sites, two groups of CV were recorded. In the first group, CVs were obtained by cycling the potential to a maximum of 0.75 V to avoid CO-oxidation in the second peak region or at higher oxidation potentials (cycles 1 and 2). The second group of CV scan (cycles 3 and 4) was carried out immediately afterwards up to a maximum of 0.9 V. It is possible to detect the disappearance of the peak at

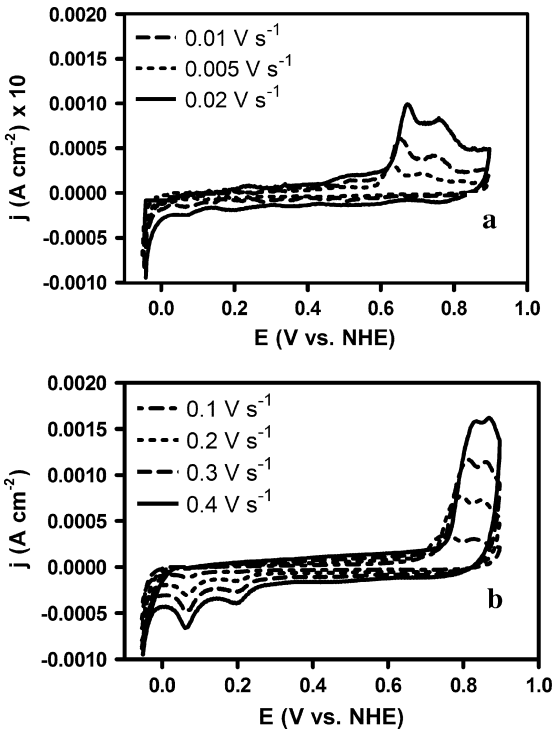

Figure 4. CO stripping voltammetry at different scan rates. In figures 4a the current density are amplified by 10 in order to better compare them, same scale range.

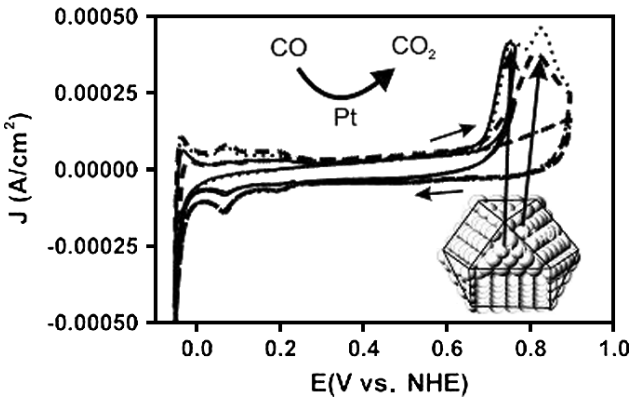

Figure 5. Stepped potential-CO-stripping experiment, 100 mV s^{-1} in 1 MH_2SO_4 solution argon purge. The sweep window was increased from 0.75 V vs. NHE (continuous line) until 0.9 V after the first two cycles (--- line). Dotted line is the complete CV going directly to 0.9 V without the pre-step at 0.75 V.

0.725 V after cycle 1, and the appearance of the lone second peak in cycle 3, which means that the first site is free of CO and that CO-oxidation proceeds only on the second site. Furthermore careful observation shows that during cycle 2 the current density in the region of the first peak is a little higher, suggesting that CO has migrated from the sites at higher energy to sites of lower energy of oxidation (i.e. from the second peak to the first). Similar results have been reported in studies on Pt (100) surfaces.[16] The first peak was preliminarily assigned as 'pre-oxidative'. In contrast, we can clearly assign the two peaks by comparison of our pattern with single-crystal studies, in the order from left to right, to oxidation of carbon monoxide adsorbed on the facets Pt(111) and Pt(100).

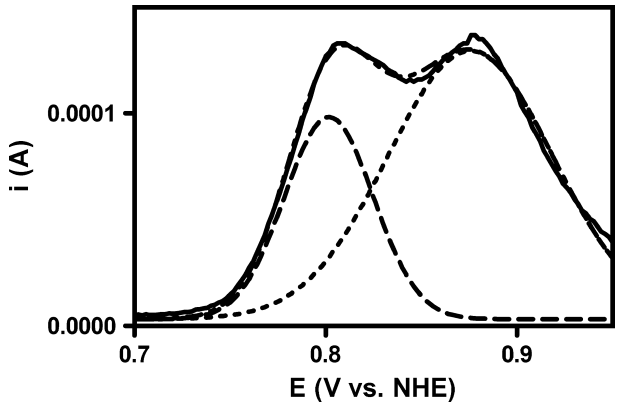

Figure 6. Decovoluted peak profile, using a double Gaussian function (Igor Pro 4.08), the CO stripping voltammograms at 300 mV s^{-1} in a 1 MH_2SO_4 solution argon purged was decomposed. (– – –) 1: Experimental peaks; (– – – –) 2: first peak and (–) 3: second peak by Gaussian function; (.–.) 4: simple sum of curves 2 and 3) .

Using the diffusion coefficients reported in Maillard *et al*.[17] (for particle sizes around 1.7 nm or 'smaller particles', $D_s \approx 10^{-16}$ cm^2 s^{-1}, and for particle sizes around 3.1 nm or 'larger particles', $D_s > 10^{-13}$ cm^2 s^{-1}) and applying Einstein's relation, the mean free path is estimated to be around 4.5×10^{-9} m s^{-1} and 1.4×10^{-10} m s^{-1}, respectively. The accuracy in the determination of the diffusion coefficients enables us to validate our hypothesis about the CO mobility in this time scale.

We also attempted deconvolution analyses of the CO-stripping peaks at five different scan rates using a double Gaussian function (*Igor Pro 4.08*; Fig. 6). By employing a deconvolution/integration routine, we obtained the distributions of CO molecules on the two different sites. The main use of this procedure is to simulate an infinitely fast scan rate, which is instrumentally unavailable, or an infinitely long relaxation time, which is experimentally inaccessible because the maximum coverage will be lost. In this figure the solid line is the experimental curve. The second and the third curves are the deconvoluted components and the fourth is their sum.

In our hypothesis, the peak at lower potential is related to thermodynamically controlled sites because it is possible, after waiting for a long time, to detect movement of CO molecules from the other kind of sites to these if they are free. At the other hand, the second CO-stripping peak can be assigned to kinetically controlled sites, or simply sites with different energies of CO-oxidation. (To confirm this it is necessary to obtain the energy of adsorptions from data at different temperatures, but they are currently unavailable. There is also another problem:[25] although the binding energy for H_{ads} is in principle calculable, in practice this is not possible because the effects of water molecules in the inner Helmholtz layer are not known sufficiently accurately, and because the adsorption of anions, i.e. SO_4^{2-}, influences the peak potentials for H adsorption.)

It is also possible to evaluate the relative coverage of these two sites at infinite scan rate, because the approximation of monolayer adsorption remains valid. At lowest potential sites related to peak 1 appear to be populated by 25% of the total adsorbed CO molecules.

To further validate our results we developed a very simple model based on O–Pt nanoparticles, based on simple calculations (see Fig. 7). In this model the following assumptions were made:

- In a cubo-octahedral nanoparticle, all the (111) planes meet each other at the corners.

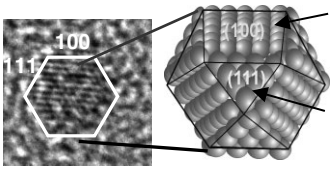

- A regular cubooctahedron has {111} and {100} surfaces.
- If seen from the (111) orientation particles will look hexagonal.
- Further, (100) surface can be considered as equivalent to square, while (111) surface is equivalent to equilateral triangle. (Vide infra)

Figure 7. Model for calculating the ration of {111} and {100} surface.

- All the sides of the cubo-octahedral particles are of equal length 'a', i.e. they are regular cubo-octahedral particles.

If we view the particle from above the (100) face, it appears to be a square shape with side length *a*, while when viewed from above the (111) surface it appears to be an equilateral triangle with side length *a*. Thus, a regular cubo-octahedral particle has eight equilateral triangular (111) faces and six square (100) faces, all of which have sides of length *a*. Considering the total area of all the (111) surfaces and (100) surfaces of the particle, the ratio area (111):area(100) is calculated to be 0.57. Atomic densities on (100) and (111) planes have been calculated previously to be 1.28×10^{15} atoms cm^{-2} for (100) faces and 1.5×10^{15} atoms cm^{-2} for (111) faces: the latter is higher owing to the close-packed hexagonal two-dimensional lattice structure. Hence the ratio of surface atoms N111:N100 is calculated to be 0.667.† [Calculating the surface area ratio of the planes (111):(100), the area of a square = area of the (100) face = a^2; the total area of the (100) planes = $6 \times a^2$; the area of an equilateral triangle = area of the (111) face = $(31/2)/4 \times a^2$; the total area of the (111) planes = $8 \times (31/2)/4 \times a^2 = 2 \times (31/2) \times a^2$; the ratio of the surface areas = A111:A100 = $2 \times (31/2) \times a^2/6a^2 = 1/(31/2) = 1/1.73 = 0.57$. The ratio of surface atoms (of the first layer) = N111/N100 = $1.5 \times 10^{15}/1.28 \times 10^{15} \times 0.57 = 0.667$ [1.5×10^{15} is the surface atomic density of the (111) plane while 1.28×10^{15} is that of the (100) planes].]

This is quite close to the ratio of 0.71 for the areas of first and second peak of the cyclic voltammogram obtained by Gaussian fit, further supporting the assignment of the peaks. If the double-peak form of the plot can be attributed to the contributions of the two different crystal planes, then the ratio of the peak areas extrapolated from the plot of the peak ratio vs 1/scan rate should be the same as the surface molar ratio of Pt(111) sites with respect to the total sites [Pt(111) + Pt(100)], which we determined to be around 0.37 (Fig. 8). However, the ratio of peak areas obtained experimentally is about 0.246 (not shown). This disagreement may arise because in the first approximation we do not take into consideration the difference between the atomic densities on the (111) and (100) crystallographic surfaces. The surface ratio extrapolated to infinite scan rate (0.246) also differs somewhat from the Kinoshita number[29] for corner and edge sites (0.22). Thus if the model actually fits the experimental results (0.667 vs 0.71), some discrepancy is present which is due to other factors. Unfortunately at the moment, due to a lack of different techniques able to double check our results, we cannot fully explain the discrepancy in the numerical ratio Pt(111)/[Pt(111) + Pt(100)]. It

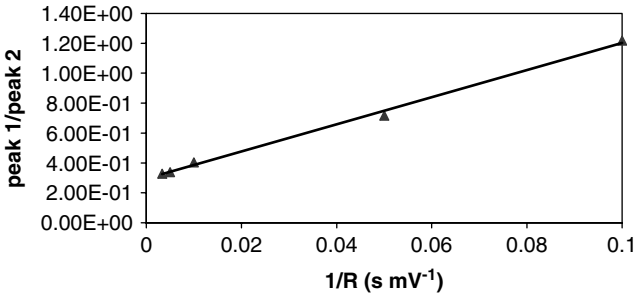

Figure 8. Peaks area calculated by integrative-deconvolutive routine, against the reverse of the sweep rates.

would be interesting to go further and look for independent experiments to study this phenomenon.

Conclusions

Previously the relationship between structure and reactivity of nanoparticles in fuel cell catalysis has only been partially established because the polycrystalline catalyst particles available had neither uniform shapes nor defined sizes. For mechanistic studies it is, however, of crucial importance to perform the experiments on well-defined nanoparticle surfaces. Via the 'seeding method', 4 nm Pt particles with controlled size and shape are accessible. Using these well-defined cubo-octahedral Pt nanoparticles having selected surface geometries, we have studied CO oxidation. CO-stripping voltammetry proves to be a very efficient and rapid method to determine the surface activity of the electrocatalysts. We observed peaks at 0.725 and 0.82V attributable to two energetically distinguishable CO-adsorption sites in cyclic voltammetry. As Marković[38] suggested, electro-oxidation of CO (from the gas phase) on Pt is highly structure-sensitive. Therefore small rearrangements of the Pt surface atoms depending upon the nanoparticle facets (111) and (100) are sufficient to affect the electronic properties of these small particles in our case. Further, we tried to model the system using simple calculations. From these results and the literature data,[6] we can identify the presence of two different types of CO molecules: type 1, which is weakly bonded on kinetically controlled adsorbing sites; and type 2, which is strongly bonded on thermodynamically controlled adsorbing sites. The ratio of weakly bonded CO to total adsorbed CO is around 0.30. This number reflects the ratio of Pt (100) atoms to the all-surface atoms, 0.22.[17] The ratio of peak areas obtained from CO-stripping voltammetry (N111:N100 = 0.667) also fits with theoretical ratio obtained by a model for surface atoms of different surfaces.

To gain information for even tentative suggestions for the mechanism, further investigations, such as FTIR, are required. The 'active site concept' proposed by Stimming and co-workers is probably the most appropriate for our systems.[17]

Acknowledgements

The authors want to acknowledge the helpful discussions of Dr E. Savinova and Dr G. N. Martelli (Industrie De Nora S.p.A, Milan, Italy) and their support during our experimental work. The contributions of Dr R. J. Mynott (Max–Planck-Institute für Kohlenforschung, Mülheim, Germany) to improving the language of this article are also gratefully acknowledged. Further, the authors want to thank by Deutsche Forschungsgemeinschaft, Bonn, Germany for financial support under grant no. 1135/2-5 (Priority Program 1060).

References

[1] Somorjai GA. *Introduction to Surface Chemistry and Catalysis*, Wiley: New York, 1994.
[2] Bradley JS. *Clusters and Colloids* (Ed.: G Schmid), VCH: Weinheim, 1994; p. 477.
[3] Ahmadi TS, Wang ZL, Green TC, Henglein A, El-Sayed AM. *Science* 1996; **272**: 1924.
[4] Narayanan R, El-Sayed MA. *J. Am. Chem. Soc.* 2004; **126**: 7194.
[5] Clint JH, Collins RI, Williams AJ, Robinson HB, Towey FT, Cajean P, Khanlodhi A. *Faraday Discuss.* 1993; **95**: 219.
[6] Fendler JH, Meldrum FC. *Adv. Mater.* 1995; **7**: 607.
[7] Murray CB, Norris DJ, Bawendi MG. *J. Am. Chem. Soc.* 1993; **115**: 8706.
[8] Brust M, Walker D, Bethell D, Schiffrin DJ, Whyman R. *J. Chem. Soc., Chem. Commun.* 1994; 801.
[9] Motte L, Billoudet F, Lacaze E, Douin J, Pileni MP. *J. Phys. Chem. B.* 1997; **101**: 138.
[10] Teranishi T, Miyake M. *Chem. Mater.* 1998; **10**: 594.
[11] Leff DV, Ohara PC, Heath JR, Gelbart WM. *J. Phys. Chem.* 1995; **99**: 7036.
[12] Bönnemann H, Brinkmann R, Britz P, Endruschat U, Mörtel R, Paulus UA, Feldmeyer GJ, Schmidt TJ, Gasteiger HA, Behm RJ. *J. New Mater. Electrochem. Syst.* 2000; **3**: 199.
[13] Bönnemann H, Nagabhushana KS. Colloidal nanometals as fuel cell catalyst precursors. In *Dekker Encyclopedia of Nanoscience and Nanotechnology* (Eds: J. A Schwarz, C.I Contescu, K Putyera), Marcel Dekker: New York, 2004; p. 739.
[14] Zurawki D, Wasberg M, Wieckowski A, *J. Phys. Chem.* 1990; **94**: 2076.
[15] Tripa CE, Yates Jr. JT. *Nature* 1999; **398**: 591.
[16] Marković NM, Lucas AC, Grgur BN, Ross PN. *J. Phys. Chem. B* 1999; **103**: 9616.
[17] Maillard F, Eikerling M, Chestiouk OV, Schrier S, Savinova E, Stimming U. *Faraday Discuss.* 2004; **125**: 357.
[18] Ross PN. *Electrochim. Acta* 1991; **36**: 2053.
[19] Kinge S, Bönnemann H. *Appl. Orgmetal. Chem.* 2006; **20**: 784.
[20] Yoo JW, Lee SM, Kim HT, El-Sayed MA. *Bull. Korean Chem. Soc.* 2004; **25**: 395.
[21] Wen F, Bönnemann H, Mynott RJ, Spliethoff B, Weidenthaler C, Palina N, Zinoveva S, Modrow H. *Appl. Organomet. Chem.* 2005; **19**: 827.
[22] Schmidt TJ, Gasteiger HA, Behm RJ. *J. Electrochem. Commun.* 1999; **1**: 1.
[23] Schmidt TJ, Gasteiger HA, Stäb GD, Urban PM, Kolb DM, Behm RJ. *J. Electrochem. Soc.* 1998; **145**: 2354.
[24] Chang SC, Weaver MJ. *J. Phys. Chem.* 1990; **94**: 5095.
[25] Wieckowski A, Rubel M, Gutiérrez C *J. Electroanal. Chem.* 1995; **382**: 97.
[26] Villegas I, Gao X, Weaver MJ. *Electrochim. Acta* 1995; **40**: 1267.
[27] Wielstich W, Gasteiger HA, Lamm A. *Handbook of Fuel Cells-Fundamentals, Technology and Applications – Fuel Cell Electrocatalysis*, Vol. 1. Wiley: New York, 2003.
[28] Schmid G. *Clusters and Colloids*. VCH: Weinhem, 1996.
[29] Kinoshita K. *Electrochemical Oxygen Technology*. Wiley: New York, 1992.
[30] Nart FC, Vielstich W. *Handbook of Fuel Cells-Fundamentals, Technology and Applications*, Wielstich W, Gasteiger HA, Lamm A. (eds), Vol. 2. Electrocatalysis, 2002; 302.
[31] Marković NM, Grgur BN, Lucas CA, Ross PN. *J. Phys. Chem. B* 1999; **103**: 487.
[32] Weaver MJ, Chang SC, Leung L, Jiang X, Rubel M, Szklarczyk M, Zurawski D, Wieckowski A. *J. Electroanal. Chem.* 1992; **327**: 247.
[33] Beden B, Lamy C, de Sacconi NR, Arvia AJ. *Electrochim. Acta* 1990; **35**: 691.
[34] Castro Luna AM, Giordano MC, Arvia AJ. *J. Electroanal. Chem.* 1989; **259**: 173.
[35] Gasteiger HA, Marković N, Ross Jr. PN, Cairns EJ *J. Phys. Chem.* 1994; **98**: 617.
[36] Chang SC, Leung L, Weaver MJ. *J. Phys. Chem.* 1989; **93**: 5341.
[37] Sasaki K, Mo Y, Wang JX, Balasubramanian M, Uribe F, McBreen J, Adzic RR. *Electrochim. Acta* 2003; **48**: 3851.
[38] Marković NM. *Surface Sci.* 1997; **384**: L805.

